Nogueira, J. J., Wang, Y., Martín, F., Alcamí, M., Glowacki, D. R., Shalashilin, D. V., Paci, E., Fernández-Ramos, A., Hase, W. L., Martínez-Núñez, E., & Vázquez, S. A. (2014). Unraveling the factors that control soft landing of small silyl ions on fluorinated self-assembled monolayers. *Journal of Physical Chemistry C*, *118*(19), 10159-10169. https://doi.org/10.1021/jp501841a

Unraveling the Factors that Control Soft Landing of Small Silyl Ions on Fluorinated Self-Assembled Monolayers

Journal:	*The Journal of Physical Chemistry*
Manuscript ID:	jp-2014-01841a.R1
Manuscript Type:	Article
Date Submitted by the Author:	n/a

Complete List of Authors:	Nogueira, Juan; University of Vienna, Institute of Theoretical Chemistry Wang, Yang; Universidad Autonoma de Madrid, Departmento de Quimica, C-9 Martin, Fernando; Universidad Autónoma de Madrid, Alcami, Manuel; Universidad Autonoma de Madrid, Quimica Glowacki, David; University of Bristol, Chemistry Shalashilin, Dmitrii; University of Leeds, Chemistry Paci, Emanuele; University of Leeds, Institute of Molecular and Cellular Biology Fernandez-Ramos, Antonio; Universidade de Santiago de Compostela, Quimica Fisica y Centro Singular de Investigación en Química Biolóxica e Materiales Moleculares (CIQUS) Hase, William; Texas Tech University, Chemistry and Biochemistry Martínez-Núñez, Emilio; Universidad de Santiago de Compostela, Departamento de Química Física, Avdas das Ciencias s/n Vazquez, Saulo; Universidad de Santiago de Compostela, Departamento de Quimica Fisica

Unraveling the Factors that Control Soft Landing of Small Silyl Ions on Fluorinated Self-Assembled Monolayers

Juan José Nogueira,[a,†] *Yang Wang,*[b] *Fernando Martín,*[b,c] *Manuel Alcamí,*[b] *David R. Glowacki,*[d] *Dmitrii V. Shalashilin,*[e] *Emanuele Paci,*[f] *Antonio Fernández-Ramos,*[a] *William L. Hase,*[g,*] *Emilio Martínez-Núñez ,*[a,*] *and Saulo A. Vázquez*[a,*]

[a]Departamento de Química Física and Centro Singular de Investigación en Química Biológica y Materiales Moleculares, Campus Vida, Universidad de Santiago de Compostela, 15782 Santiago de Compostela, Spain.
[b]Departamento de Química, Universidad Autónoma de Madrid, Cantoblanco, 28049 Madrid, Spain
[c]Instituto Madrileño de Estudios Avanzados en Nanociencia (IMDEA Nanociencia), Cantoblanco, 28049 Madrid, Spain
[d]School of Chemistry, University of Bristol, Bristol BS8 1TS, United Kingdom
[e]School of Chemistry, University of Leeds, Leeds LS2 9JT, United Kingdom
[f]Institute of Molecular and Cellular Biology, University of Leeds, Leeds LS2 9JT, United Kingdom
[g]Department of Chemistry and Biochemistry, Texas Tech University, Lubbock, Texas 79409-1061, USA.

Corresponding Authors: William L. Hase (bill.hase@ttu.edu), Emilio Martínez-Núñez (emilio.nunez@usc.es), and Saulo A. Vázquez (saulo.vazquez@usc.es).

[†]Present address: Institute of Theoretical Chemistry, University of Vienna, Währinger Str. 17, 1090 Vienna, Austria.

Abstract

Dynamics simulations were performed to study soft landing of $SiNCS^+$ and $(CH_3)_2SiNCS^+$ ions on a self-assembled monolayer of perfluorinated alkanethiols on gold (F-SAM). Using classical trajectories, the short-time collision dynamics (ps scale) were investigated to analyze trapping probabilities for these silyl ions. Thermal desorption of trapped ions was simulated by using "boxed molecular dynamics" (BXD). The simulations predict substantial ion trapping in the collisions of these ions with the F-SAM, especially when the projectile's incident direction is normal to the surface. Desorption of the $SiNCS^+$ ion occurs significantly faster than desorption of the methylated ion, which may explain why soft landing was experimentally observed for the latter ion only [Miller, S. A.; Luo, H.; Pachuta, S. J.; Cooks, R. G., *Science* **1997,** *275*, 1447-1450; Luo, H.; Miller, S. A.; Cooks, R. G.; Pachuta, S. J., *Int. J. Mass. Spectrom. Ion Proc.* **1998,** *174*, 193-217]. The free energy profiles for desorption of these ions show minima at 15 Å above the gold slab, indicating that the silyl ion has a preference to reside on top of the monolayer. Deep penetration of the ion into the monolayer is prevented by a large free energy barrier. However, according to DFT calculations, if this process occurred the $SiNCS^+$ ion could strongly bind to the Au(111) surface that supports the perfluorinated alkanethiol chains.

Keywords: Soft landing, self-assembled monolayers, silyl ions, classical trajectory calculations, molecular dynamics simulations, accelerated dynamics.

Introduction

Ion/surface collisions may lead to a variety of competing processes that can be used to investigate the chemical nature of projectile ions and target surfaces.[1] At hyperthermal energies (<100 eV), the most relevant events that can take place when ions collide with molecular surfaces are:[1-2] (i) non-reactive scattering of the projectile ion, (ii) surface-induced dissociation (SID), (iii) ion/surface reactions, (iv) sputtering, (v) soft landing, and (vi) reactive landing. The term sputtering refers to processes in which the collision induces the ejection of surface species. This includes pre-existing ions adsorbed on the surfaces as well as fragments of molecular units that form the surface. Soft landing (SL) is used to name the deposition of intact ions on target surfaces, with or without retention of the initial charge.[3-11] Reactive landing (RL) takes place when a covalent bond is formed between the landed ion and the surface. The main factors that govern the efficiencies of these processes are the physical and chemical properties of the surface, the nature of the ion, the collision energy, and the incident angle. For low collision energies (on the order of 10 eV), SL may be the dominant process. The first SL experiments were reported in 1977 by Cooks and co-workers,[12] but it was not until the late 1990's that it began to receive significant attention when it was proposed as a practical method for preparing modified surfaces.[13] The advantage of SL over other methods of preparation of materials resides in the high selectivity of the projectile ion (chemical, isotopic, structural) together with some control over the collision process through the selection of the projectile translational energy.[1, 14-15]

The kind of projectile ions that have been used in SL studies include small and medium size polyatomic ions,[12-13, 16-21] atomic and organometalic clusters,[22-24] peptides,[5, 21, 25-30] proteins,[26, 31-35] DNA,[36] and even viruses.[37] Among the molecular surfaces employed as targets,

self-assembled monolayers (SAMs) of alkanethiolates on gold[38] have been the most widely used for several reasons.[1] They can be prepared with low levels of surface contamination, they are stable in ultrahigh vacuum conditions, and have a well-characterized and highly ordered structure, therefore making them excellent candidates for fundamental studies. In addition, the ease with which the terminal groups of the chains can be functionalized by different chemical species opens a wide variety of possibilities for the design of novel materials.

In collisions of silyl ions with a perfluorinated alkanethiol self-assembled monolayer on gold (F-SAM), bombardment of an F-SAM surface for 1 h with $(CH_3)_2SiNCS^+$ and subsequent bombardment with 60 eV Xe^+ ions led to a peak at *m*/*z* 116 (i.e., the *m*/*z* ratio of this silyl ion) in the sputtering spectrum.[13, 16, 39] This peak was also observed when the bombarded F-SAM was kept in the scattering chamber under vacuum for 15 h, although the relative intensity dropped by a factor of two. These results were interpreted as an evidence for soft landing with charge retention,[13, 16] and were observed for collision energies, E_i, in the range of 5-10 eV and an incident angle, θ_i, of 0º (i.e., normal to the surface), as well as for E_i = 20 eV and incident angles of 0 and 55º. Interestingly, when the collision energy was 30 eV and the incident angle was 55º, the sputtering spectrum did not show the peak at *m*/*z* 116. On the other hand, when $SiNCS^+$ was collided with the F-SAM surface (E_i = 5-10 eV and θ_i = 0º), the subsequent sputtering spectra did not show a peak for this ion, suggesting that SL did not occur for this species. Analyses of the sputtering spectra obtained from different Xe^+ collision energies led Cooks and co-workers[16] to conclude that the $(CH_3)_2SiNCS^+$ ion is relatively strongly trapped in the surface, and that the methyl groups may increase the attractive interaction with the monolayer and facilitate trapping of the ion by the disturbed perfluoroalkane chains.[13, 16]

To gain some insight into the mechanisms that govern soft landing of small polyatomic ions on SAM surfaces, we report an investigation on the short-time dynamics of collisions of the $SiNCS^+$ and $(CH_3)_2SiNCS^+$ ions with an F-SAM surface, and the subsequent long-time desorption dynamics of trapped ions. The key questions addressed in this work are: (1) Are the trapping probabilities for the $SiNCS^+$ and $(CH_3)_2SiNCS^+$ ions very different from each other? And how do they vary with collision energy and incident angle? (2) How different are the ion-surface interaction energies for these two ions? (3) Is the observed behavior (i.e., soft landing only for the methylated ion) the consequence of significant differences between time scales for ion desorption? (4) Can deep penetration into the monolayer and subsequent ion neutralization (by electron transfer from the Au surface) be important for these ions?

The short-time (ps scale) dynamics is investigated here by classical trajectories, characterized by the values of the collision energy and incident angle. Trapping will occur when a substantial fraction of the collision energy is transferred to the monolayer and to the internal modes of the ion, so that there is not enough recoil translational energy for the ion to escape. Eventually (in the ps scale), the excited modes in the ion and in the surrounding region will dissipate the excess energy and reach thermal equilibrium at the surface temperature. Since the experiments show that $(CH_3)_2SiNCS^+$ ions remain trapped in the F-SAM for days, [13, 16] an "accelerating" technique is needed to conduct molecular dynamics of desorption of these ions from the F-SAM. In this work, we employed "boxed" molecular dynamics,[40-42] a convenient method for accelerating rare events, which is outlined in the following section together with the remaining computational details of the simulations reported in this paper.

Computational details

Analytical potential. The potential energy function (or force field) used for the dynamics simulations reads

$$V = V_{silyl} + V_{surf} + V_{silyl-surf} \quad (1)$$

where V_{silyl} is the intramolecular potential of the silyl ion, V_{surf} is the intramolecular potential of the F-SAM,[43-44] and $V_{silyl-surf}$ is the interaction potential between the silyl ion and the surface.[45] The intramolecular potentials V_{silyl} were developed in this work. For the smallest ion, it is given by a sum of harmonic stretches and bends:

$$V_{silyl} = \sum_i \frac{1}{2} k_s (r - r_0)^2 + \sum_i \frac{1}{2} k_\theta (\theta - \theta_0)^2 \quad (2)$$

where the force constants k_s and k_θ were obtained by a fit to normal mode vibrational frequencies calculated by density functional theory (DFT), using the B97-D method[46-47] and the TZVPP basis set, as implemented in TURBOMOLE.[48] The r_0 and θ_0 parameters were taken from the DFT equilibrium geometry and are listed in Table S1 in the Supporting Information. The comparison between the DFT frequencies and those calculated with the analytical potential is shown in Table S2.

The intramolecular potential function of the $(CH_3)_2SiNCS^+$ ion requires torsional terms and an out-of-plane wag term besides stretching and bending interactions. The Si-C stretching interactions were represented by Morse functions and the other stretches by harmonic functions. Accordingly, the intramolecular potential for the $(CH_3)_2SiNCS^+$ reads

$$V_{ion} = \sum_{i \neq Si-C} \frac{1}{2} k_s (r - r_0)^2 + \sum_{i=Si-C} D_e \left(1 - e^{-\beta(r-r_0)}\right)^2 + \sum_i \frac{1}{2} k_\theta (\theta - \theta_0)^2 + \sum_i \frac{1}{2} k_\alpha (\alpha - \pi)^2 + \sum_i \sum_n \frac{1}{2} k_{t,n} (1 + \cos(n\varphi - \gamma_n)) \quad (3)$$

where the force constants for the wag, bends, and torsions involving the Si-C bonds include a switching function that removes these potential terms as a Si-C bond breaks:

$$k_\theta = k_\theta^0 s_{AB} s_{BC} \quad (4)$$

$$k_\alpha = k_\alpha^0 s_{AB} s_{AC} s_{AD} \quad (5)$$

$$k_t = k_t^0 s_{AB} s_{BC} s_{CD} \quad (6)$$

In these equations, the superscript 0 is used to indicate conventional force constants, and the s_{ij} refer to switching functions depending on the distance between atoms *i* and *j*, having the form

$$s_{ij} = e^{-c_{ij}(r_{ij}-r_0)^2}, \ r_{ij} \geq r_0$$

$$s_{ij} = 1.0 \ \ r_{ij} < r_0 \quad (7)$$

with c_{ij} being set to 0.1 for all cases. The use of this type of switching functions has been described elsewhere.[49] Figure 1a displays the different interactions that include this switching function. The second term in equation 3 corresponds to the Morse potentials for the Si-C bonds. D_e is the equilibrium dissociation energy. The first and the second dissociation energies were calculated in this work by Gaussian-4 theory,[50] and are shown in Figure 1b. An attenuation function was included to smoothly switch from $D_{e,1}$ (98.98 kcal/mol) to $D_{e,2}$ (39.50 kcal/mol) as a methyl group dissociates:

$$D_e = D_{e,1} + \left(D_{e,2} - D_{e,1}\right)\frac{1}{2}(1 + \tanh(\bar{R}_{Si-C} - C)) \quad (8)$$

where $\bar{R}_{\mathrm{Si-C}}$ is the average Si-C bond length. *C* was set to 5 Å, the distance at which $D_e = (D_{e,1}+D_{e,2})/2$. The r_0 and θ_0 parameters were taken from the B97-D/TZVPP equilibrium geometry, and the force constants were obtained by a fit to B97-D/TZVPP frequencies. The parameters and the comparison between the DFT frequencies and those calculated with the analytical potential are shown in Tables S3 and S4, respectively, in the Supporting Information.

The intramolecular potential for the F-SAM, V_{surf}, is based on a force field of perfluoroalkanes developed by Borodin et al.[51] It comprises of harmonic terms for stretching and bending interactions, cosine series for dihedrals, and Buckingham-type potentials[52] for nonbonded interactions. The F-SAM surface is composed of 48 chains of $CF_3(CF_2)_7S$ adsorbed on a fixed Au layer of 225 atoms. A full description of the F-SAM model has been detailed in the literature.[43-44]

The intermolecular term, $V_{silyl\text{-}surf}$, is written as a sum of two-body functions based on the Buckingham potential:[52]

$$V = \sum_i \sum_j \left\{ A e^{-B r_{ij}} + \frac{C}{r_{ij}^D} + \frac{E}{r_{ij}^F} \right\} \quad (9)$$

where subscripts *i* and *j* refer to atoms of the silyl ion and the F-SAM, respectively. For each ion, parameters *A* to *F* were obtained in previous work[45] by a fit to potential energy curves of CF_4 interacting with the ion, calculated at the B97-D/TZVPP level. The good performance of this DFT method was tested, for the $SiNCS^+$ ion, by a comparison with interaction curves determined by focal point CCSD(T) calculations. As in previous parameterizations of gas/F-SAM intermolecular potentials,[43, 53-59] CF_4 was used as a model compound for the C and F atoms of perfluoroalkane chains. The fitted potentials were shown to model quite well the potential energy curves calculated by B97-D/TZVPP for the silyl ions approaching nine molecules of perfluorobutane.[45]

Short-time collision dynamics. We used the Venus program[60-61] to explore the dynamics of collisions of the silyl ions with the F-SAM and the evolution of the system during the subsequent picoseconds. We prepared ensembles of trajectories for collision energies of 10 and 30 eV, and incident angles of 0º and 55º. The incident angle is defined as the angle formed between the

initial velocity vector of the projectile ion and the surface normal. In these simulations, the zero-point energy (ZPE) was added to the normal modes of the silyl ion, and the total rotational angular momentum of the projectile was set to zero. The temperature of the F-SAM was set to 300 K. We notice that the experiments of Cooks and co-workers[13, 16, 39] were carried out at room temperature.

For each different pair of E_i and θ_i values, ensembles of 2000 trajectories were propagated with a fixed time step of 0.3 fs, using the Adams-Moulton algorithm in VENUS05.[60] The initial separation between the projectile and the surface aiming point was 40 Å (≈52 Å above the gold atoms). Trajectories were stopped when the total integration time exceeded 60 ps or when the distance between the ion and the surface was 45 Å. Before the beginning of the trajectory simulations, the surface was thermally equilibrated by a 2ps trajectory in which the atomic velocities were scaled every 100 time steps to fit a Maxwell-Boltzmann distribution at 300 K. This structure was used as the initial configuration for the first trajectory. A second 100 fs equilibration run, starting from the previous configuration (i.e., the F-SAM configuration for the first trajectory at time t = 0), was performed before the second trajectory. This process was repeated before initiation of each trajectory. Periodic boundary conditions based on the image vector convention[62] were used for the simulations.

Long-time desorption dynamics. The simulations performed to estimate time scales for desorption of silyl ions were conducted with boxed molecular dynamics (BXD),[40-42] utilizing a new reaction coordinate implemented in the CHARMM program.[63-64] This new routine allows the user to arbitrarily define a group of atoms, track their mass weighted separation in the Cartesian z-direction, and perform velocity inversion for the appropriate z-components of the

atomic velocity. The basis of the BXD method for a general reaction coordinate or progress parameter is illustrated in Figure 2, which shows the reaction coordinate ρ split into m intervals or boxes. The trajectory is initiated in one of them (e.g., box 1) and confined in the box by velocity inversion along the reaction coordinate each time the system hits the boundaries. After a given number of hits, the trajectory is allowed to enter into the neighboring box where, again, it is locked until the specified number of hits is reached. The process is repeated until the end of the trajectory. The rate coefficient for passage from box i–1 to box i is given by the ratio between the number of hits against the boundary at ρ_i and the lifetime of the trajectory in box i, that is, the inverse of the mean first passage times (MFPTs). Since rate coefficients are related to equilibrium constants and free energies, BXD also provides thermodynamic information through the following relationship:

$$K_{i-1,i} = \frac{k_{i-1,i}}{k_{i,i-1}} = \exp\left(-\frac{\Delta G_{i-1,i}}{RT}\right) \tag{10}$$

where $k_{i-1,i}$ is the rate coefficient for transfer from box i–1 to box i and $k_{i,i-1}$ is the rate coefficient for the reverse process; $K_{i-1,i}$ and $\Delta G_{i-1,i}$ are the equilibrium constant and the free energy difference between the boxes, respectively. As detailed elsewhere,[40-42] it is possible to define smaller bins within boxes and obtain box-to-box rate coefficients and corresponding free energies with higher resolution.

Once the box-to-box rate coefficients are obtained, the time evolution of the system can be determined from the following set of simultaneous first-order linear differential equations:

$$\frac{dn_1(t)}{dt} = -k_{1,2}n_1(t) + k_{2,1}n_2(t)$$

.....

$$\frac{dn_i(t)}{dt} = k_{i-1,i}n_{i-1}(t) + k_{i+1,i}n_{i+1}(t) - \left(k_{i,i-1} + k_{i,i+1}\right)n_i(t) \tag{11}$$

.....

$$\frac{dn_m(t)}{dt} = k_{m-1,m}n_{m-1}(t) - k_{m,m-1}n_m(t)$$

where $n_i(t)$ gives the population of box i at time t. This set of equations can be conveniently written in matrix form

$$\frac{d\mathbf{n}(t)}{dt} = \mathbf{M}\mathbf{n}(t) \quad (12)$$

where **n**(t) is the population vector and **M** is the matrix of the rate coefficients. The general solution to this equation is given by[65]

$$\mathbf{n}(t) = \sum_{j=1}^{m} c_j \mathbf{u}_j e^{\lambda_j t} \quad (13)$$

where λ_j and $\mathbf{u}_j$ are the eigenvalues and corresponding eigenvectors of **M**, and the c_j are coefficients that depend upon the initial populations **n**(0). In this work, we used the initial populations given by a thermal distribution at 300 K. Within the approximations of classical dynamics and the model potential energy used for the simulations, the calculation of the above quantities is accurate so long as the dynamics of the system is statistical and the trajectory visits all the relevant phase space. In practice, one may run independent trajectories, analyze the convergence of results, and run new trajectories if necessary.

For the present simulations, the reaction coordinate was defined as the distance (or height) of the center-of-mass of the silyl ion to the gold layer (h), and it was split into 44 boxes of 0.5 Å length, ranging from 8 to 30 Å. Free energies were determined with a resolution of 0.1 Å length. The simulations were conducted with Langevin dynamics at 300 K, using a time step of 1 fs and a friction coefficient of 5 ps^{-1}, which was the minimal friction coefficient we found to give satisfactory temperature profiles. Because the non-bonded interactions of the analytical potential used in this work are modeled by functions based on the Buckingham potential, rather

than by Lennard-Jones potentials and point-charge electrostatic interactions, the CHARMM program was modified to incorporate these generalized Buckingham terms. For these long-time dynamics simulations, the C-Si bonds of the $(CH_3)_2SiNCS^+$ ion were represented by harmonic functions, and the F-SAM surface consisted of 108 chains of $CF_3(CF_2)_7S$ adsorbed on a layer of 441 fixed Au atoms. As for the short-time collision dynamics, two-dimensional rhomboidal periodic boundary conditions were applied in the simulations.[62]

The force field used for our simulations did not incorporate an interaction term between the ion and the Au surface. This interaction may be relevant for the calculation of desorption rates. The development of an accurate potential for this interaction would be a very involved task, and it was not done in the present study. However, we used a simple approach with which we could integrate, in an approximate way, the effect of the ion/Au surface interaction in the free energies and box-to-box rate coefficients. The approach is based on the classical point charge/metal surface expression, which reads[66]

$$V^{ip} = -\frac{83.02}{\varepsilon h} \qquad (14)$$

where the potential energy is given in kcal/mol, ε is the dielectric constant and h is the distance of the silicon atom to the Au surface. We assumed that all the ion charge is located on the Si atom, as the B97-D/TZVPP calculations show that most of the charge is concentrated on this atom. We used ε = 1.55, which is the mean value between the dielectric constant of polytetrafluoroethylene[67] and that of vacuum. BXD simulations including this charge image potential would be very time consuming, because the range of this interaction is very long (using equation 14, the interaction energy at 100 Å is still about 0.5 kcal/mol). Instead, we used the following approximation to calculate box-to-box rate coefficients, $k_{i-1,i}^{ip}$, that contain the effect

of this potential. We assumed that, in the presence of the image potential, the free energy difference between neighboring boxes *i*–1 and *i*, $\Delta G^{ip}_{i-1,i}$, can be approximated by

$$\Delta G^{ip}_{i-1,i} = \Delta G_{i-1,i} + \Delta V^{ip}_{i-1,i} \quad (15)$$

where $\Delta V^{ip}_{i-1,i}$ is the difference between the values of the image potential calculated in the midpoints of the *i*–1 and *i* boxes. Now, following equation 10, we have

$$\frac{k^{ip}_{i-1,i}}{k^{ip}_{i,i-1}} = \exp\left(-\frac{\Delta G^{ip}_{i-1,i}}{RT}\right) = \frac{k_{i-1,i}}{k_{i,i-1}}\exp\left(-\frac{\Delta V^{ip}_{i-1,i}}{RT}\right) \quad (16)$$

The image potential varies only slightly from box to box, so that it is a reasonable approximation to assign half of ΔV^{ip} to each of the boxes. Accordingly, the individual rate coefficients are calculated as:

$$k^{ip}_{i-1,i} = k_{i-1,i}\exp\left(-\frac{\Delta V^{ip}_{i-1,i}}{2RT}\right) \quad (17)$$

and

$$k^{ip}_{i,i-1} = k_{i,i-1}\exp\left(+\frac{\Delta V^{ip}_{i-1,i}}{2RT}\right) \quad (18)$$

Density functional theory (DFT) calculations. We also investigated the close interaction between the silyl ions and the Au surface to consider the possibility that the ion penetrates deeply into the monolayer and approaches the Au surface. To this end, we performed DFT calculations using the generalized gradient approximation (GGA) for the exchange-correlation functional of Perdew, Burke, and Ernzerhof (PBE),[68] implemented in the Vienna ab initio simulation package (VASP).[69-71] To describe the effective potential of the core electrons, the projector-augmented

wave (PAW) method[72-73] was utilized. A cutoff energy of 450 eV for the plane wave expansion and a Methfessel Paxton smearing[74] of 0.2 eV for the occupation of electronic states were chosen. The Brillouin-zone sampling was performed with a 3 x 3 x 1 k-point mesh according to the Monkhorst-Pack grid.[75]

The Au(111) surface was modeled by a four-layer slab cut from the bulk crystal whose structure was optimized beforehand. The gold slab, which consisted of 12 atoms per layer, and the ion were placed in a 3-dimensional periodic cell separated by ≈ 23 Å of vacuum in the surface normal direction. In order to simulate a positively charged molecule on the Au(111) surface, a uniform negative background compensation charge was introduced to maintain the charge neutrality of the unit cell. During the geometry optimizations, the lowermost two layers of the Au(111) surface were frozen, while the topmost two layers and the whole molecule were fully relaxed. The local minimum of potential energy was searched by a conjugate-gradient algorithm until the forces on each ion were smaller than 0.02 eV $Å^{-1}$. Different initial configurations were explored in order to determine the most favorable adsorption sites. The atomic charge distribution was computed by the topological analysis of the electron density (including the core charge), based on the quantum theory of atoms in molecules (QTAIM)[76-78] and using an analysis program[79] for VASP.

Results and discussion

Short-time collision dynamics. Trajectories were classified according to the values of the following quantities: the minimum distance (or height h) of the projectile center-of-mass to the Au plane, h_{min}, the number of inner turning points (ITPs) in the direction of the surface normal that the ion experiences during the collision, and the time interval during which the ion interacts

with the surface. Specifically, we considered that the projectile ion penetrates into the monolayer when the height of the ion is below 11.6 Å. This limiting distance (h_{limit} in Figure 3) was calculated as the average value $0.5\langle h_{\mathrm{CF_3}} + h_{\mathrm{CF_2}}\rangle$, where $h_{\mathrm{CF_3}}$ is the height of the C atom of the methyl group of an F-SAM chain and $h_{\mathrm{CF_2}}$ is that of the adjacent C atom. For this calculation, we used a structure obtained by a short molecular dynamics simulation of the monolayer at 300 K. Two types of penetrating trajectories were identified in the simulations: (i) trajectories in which the ion penetrates directly with no ITPs (direct-penetration), and (ii) trajectories in which ion penetration occurs after two or more ITPs (physisorption-penetration). The other types of trajectories are non penetrating, and include (iii) direct scattering, when the ion rebounds after collision with only one ITP, and (iv) physisorption, when the collision takes place with two or more ITPs. Figure 4 shows schematic drawings for trajectory types (ii)-(iv). Finally, for a significant number of trajectories, the ion does not leave the surface during the 60 ps of integration. This type of trajectories will be referred to as trapped. Notice that trapped trajectories may involve physisorption and penetration but not direct scattering, and that the sum of trajectory types (i) to (iv) add up to 100%. The amount of trapped trajectories may be different to the sum of penetrating and physisorbing trajectories (the difference is due to the fraction of these trajectories that leave the monolayer before 60 ps). After 60 ps, one may expect that most of the excitation energy in the collision region was dissipated to the F-SAM and so that thermal equilibrium is essentially reached. Therefore, we may associate trapping with soft landing in a short-time, picosecond scale.

The percentages of the different types of trajectories are listed in Table 1. As can be seen, when the incident angle is 0º, most of the trajectories lead to direct penetration. However, when the angle increases to 55º, the percentage of this type of trajectories decreases dramatically,

being less than 5 and 20% for the collision energies of 10 and 30 eV, respectively. This behavior was also found for collisions of atomic oxygen with an alkanethiol self-assemble monolayer;[80] interestingly, some of the O-atoms approached the Au substrate. For θ_i = 55º, the majority of trajectories resulted in physisorption (10 eV) or physisorption-penetration (30 eV). Also, the percentage of direct scattering increases when going from θ_i = 0º to 55º. We notice that the criterion for classification of trajectories, particularly the selection of h_{limit}, is somewhat arbitrary. Clearly, there is no universal way to classify trajectories and here we followed the same criteria employed in previous studies of collisions of gases with an F-SAM.[43, 58, 81] The percentages of different trajectory types may change significantly with the value of h_{limit}, as shown in Table S5 of the Supporting Information for the case of E_i = 10 eV and θ_i = 0º.

It is important to analyze the percentage of trajectories in which the ion remains trapped in the surface after the total integration time of 60 ps. For the collision energy of 10 eV, more than 80% of the trajectories are trapped in the monolayer when θ_i = 0º. When the incident angle is 55º (and E_i = 10 eV), the percentage of trapped trajectories decreases substantially, especially for the small ion (15.7%). For E_i = 30 eV and θ_i = 0º, the percentage of trapping is also substantial (around 70%). Again, as the incident angle increases to 55º, the percentage of trapped trajectories decreases markedly, although the percentage of trapping is still significant (e.g., 9.1 % for $(CH_3)_2SiNCS^+$). Since soft landing of $(CH_3)_2SiNCS^+$ was not observed experimentally for E_i = 30 eV and θ_i = 55º, these results suggest that our potential may overestimate the trapping probabilities.

The simulations predict more trapping for the $(CH_3)_2SiNCS^+$ ion, except for E_i = 30 eV and θ_i = 55º. This is a result of the extra vibrational modes in the methylated species, compared with $SiNCS^+$, which facilitate more energy transfer from relative translational energy to

vibration, therefore leading to less energy in final translation. At the incident energy of 10 eV and for perpendicular collisions, the percent of energy transfer to vibration is 6.6% for $SiNCS^+$, compared with 14.4% for $(CH_3)_2SiNCS^+$ (see Table S6). This result can be explained with a model for gas-surface energy transfer proposed very recently by three of us.[82] The model shows that, for small projectiles like those studied here, transfer to vibration increases as a function of projectile's size. For larger projectiles, however, transfer to vibration would be nearly constant and independent on the projectile's size. This is because the increase in the number of vibrational degrees of freedom is offset by a mass effect and by the previous finding that only a reduced subset of "effective" vibrational degrees of freedom is activated in the collisions.[82] The most relevant result of this section is that the simulations predict that the general behavior of both ions is quite similar to each other.

Long-time desorption dynamics. Our simulations of short-time dynamics of collisions of silyl ions with the F-SAM monolayer predict that soft landing is likely for both ions. The experimental observation that only the methylated species is observed in the sputtering analysis could be explained if the thermal desorption of the two ions takes place on significantly different time scales. One of the advantages of the BXD method with respect to other common sampling methods, for example, umbrella sampling,[83] is that it provides kinetic information in addition to thermodynamic properties. The box-to-box rate coefficients, calculated as the inverse MFPTs, are collected in Tables S7 and S8 for $SiNCS^+$ and $(CH_3)_2SiNCS^+$, respectively. First passage times (FPTs) were corrected to remove fast recrossing events along the reaction coordinate, and the tables include both uncorrected coefficients and corrected values using a decorrelation time, τ_{corr}, of 125 fs. In the later case, FPTs smaller than 125 fs were not included in the count for the evaluation of the MFPTs. The value of 125 fs was chosen as the maximum decorrelation time

which did not significantly affect the resultant box averaged probabilities, a procedure which was described in previous work.[41] The kinetic equations resulting from the box-to-box rate coefficients gave solutions in which one of the eigenvalues was distinct from the others by several orders of magnitude. In such cases, this so-called 'chemically significant' eigenvalue dominates the sum of equation 13 and gives the characteristic rate constant of the chemical process under investigation,[84] that is, the desorption of the silyl ions in the present study. According to our calculations without including the effect of the image potential, the rate constants for desorption of the $SiNCS^+$ and $(CH_3)_2SiNCS^+$ ions from F-SAM at 300 K are 4.3×10^4 and 8.5×10^2 s^{-1}, respectively. Therefore, the $SiNCS^+$ ion desorbs about 50 times faster than the methylated ion. The residence times of these ions, that is, the inverse of the rate constants, are 2.3×10^{-5} and 1.2×10^{-3} s, respectively. The experiments suggest that this ion remains trapped in the F-SAM for hours, and even days, raising the prospect that our simulations underestimate the timescale for desorption of the methylated ion.

The main source of error in our results probably arises from inaccuracies of the analytical potential. For example, the intramolecular potentials of the silyl ions were determined from vibrational frequencies and equilibrium geometries for the isolated ions. Therefore, these potentials may not be sufficiently accurate when the ions interact strongly with the surface, particularly during the short-time collision event and when the ion is inside the monolayer, since the structure of the ion could be highly altered. Also, as mentioned before, the force field used for the simulations did not include an interaction term with the Au surface. Including the effect of the charge image potential, as described in the section on computational details, the rate constants for desorption are calculated to be 0.66 s^{-1} for $SiNCS^+$ and 1.1×10^{-2} s^{-1} for $(CH_3)_2SiNCS^+$. We notice that slight changes in the dielectric constant would affect the rate

constants substantially. These values give residence times of about 1.5 s for the $SiNCS^+$ ion and 91 s for the methylated species. Although the residence time of the latter ion is short in comparison with the experimental observation (i.e., the ion remains trapped for days), the qualitative picture provided by our simulations is that the $SiNCS^+$ ion desorbs significantly faster than the $(CH_3)_2SiNCS^+$ ion. A rapid desorption of the $SiNCS^+$ ion may be the reason why this ion is not observed in the experiments.

Figure 5 depicts the free energy profiles computed with the BXD approach for desorption of the $SiNCS^+$ and $(CH_3)_2SiNCS^+$ ions, respectively, at 300 K. As mentioned before, the reaction coordinate ρ corresponds to the distance of the center-of-mass of the silyl ion to the Au surface (i.e., $\rho = h$). The simulations show that desorption takes place with no reverse barrier. For the $SiNCS^+$ ion, the simulations (without the image potential) predict a desorption free energy, ΔG_{des}, of 7.9 kcal/mol at 300 K. Using the image potential approximation, $\Delta G_{\text{des}}^{ip}$ is estimated to be 11.0 kcal/mol. Notice that for the free energies obtained with the image potential approximation, the graph only shows the curves up to 30 Å, so that it is necessary to add to the free energy value at 30 Å a contribution of 1.3 kcal/mol (i.e., ΔG from 30 Å to infinity). For the methylated ion, ΔG_{des} at 300 K is predicted to be 10.3 kcal/mol, without the image potential, and 13.4 kcal/mol with the charge image potential. Therefore, desorption of the methylated ion is about 2.4 kcal/mol more endergonic than desorption of the parent species. The global minima of the curves are located close to 15 Å, which indicates a preference for the ion to reside on (not inside of) the surface. However, the simulations predict that the most attractive interactions between these ions and the F-SAM, about –30 and –40 kcal/mol for $SiNCS^+$ and $(CH_3)_2SiNCS^+$, respectively, occur when the ion is inside the monolayer, at a distance of ≈ 8 Å relative to the Au surface. These values were obtained from analyses of molecular dynamics trajectories (one for

each ion), starting each trajectory from a configuration in which the ion was located at about 7 Å, and using BXD to accelerate the desorption. The value of 8 Å is close to the estimate of Cooks and co-workers for the $(CH_3)_2SiNCS^+$ ion (≈7 Å).[16] As they anticipated, the attractive interactions are stronger for the methylated ion. It is the entropic contribution, favorable for desorption, which makes, according to our simulations, the top of the monolayer as the most favorable place for the ion to be located.

Interaction with the Au surface. Although our simulations predict that deep penetration into the F-SAM is difficult, since the free energies increase significantly as the ions penetrate into the monolayer, the possibility that the ions approach the Au(111) surface and get neutralized or strongly chemisorbed should not be completely disregarded. If this happened to the $SiNCS^+$ ion, the sputtering spectra might not reveal the existence of this ion in the monolayer. An accurate investigation on the interactions of the $SiNCS^+$ and $(CH_3)_2SiNCS^+$ ions with the gold surface, including the perfluoroalkane chains, is impractical with the present computational resources. Instead, we performed DFT calculations to evaluate binding energies for chemisorption of $SiNCS^+$ and $(CH_3)_2SiNCS^+$ ions on a Au(111) surface, as well as to explore the possibility of neutralization of the ion. As described above, the geometries of the whole ion and that of the topmost two gold layers were fully relaxed. The calculations predict that the $SiNCS^+$ ion chemisorbs on Au(111) in a hollow face-centered cubic (fcc) site, with an orientation parallel to the surface normal, as depicted in Figure 6. The Si atom binds to three Au atoms, with a total binding energy of 60.0 kcal/mol (20 kcal/mol per bond), which is somewhat higher than the estimated bond strength for the Au–S links (≈ 50 kcal/mol).[38] The distance between the Si atom and each of the closest Au atoms is predicted to be 2.38 Å. The $SiNCS^+$ ion can also bind to only

one Au atom in an atop site, but this arrangement is less stable than that involving a hollow fcc site by 39.2 kcal/mol (i.e., by about 2/3 of the total interaction energy in the fcc binding).

For $(CH_3)_2SiNCS^+$/Au(111), the Si goes to an atop site and binds to only one gold atom. The binding energy is 30.0 kcal/mol and the Si-Au bond length is 2.46 Å. As shown in Figure 6, the geometry of the ion is significantly distorted from its gas phase structure. Contrary to the $SiNCS^+$/Au(111) system, in this case the ion is oriented parallel to the surface. In an F-SAM monolayer, the fluorinated alkanethiol chains would probably prevent the ion from binding to the gold surface in this form. On the other hand, the binding energy for an orientation in which the $(CH_3)_2SiNCS^+$ ion approaches the Au(111) surface perpendicularly, through an S atom attack, is very small (0.7 kcal/mol). Therefore, the probability for strong binding is negligible for this ion.

Using QTAIM,[76-78] we calculated atomic charges (core electron densities were included) for the ions bound to the Au surface. As shown in Figure 6, the Si atom has, in both cases, the largest positive charge, 1.76 and 2.51 au for $SiNCS^+$ and $(CH_3)_2SiNCS^+$, respectively. It is important to notice that the total charge on the small ion is quite large (+1.12 au), and significantly larger than that on the methylated ion (+0.62 au). This result may suggest that neutralization of these ions is very unlikely, especially for $SiNCS^+$. To sum up, the results presented in this section open the possibility of an alternative mechanism that might also explain the experimental observations: deep penetration of the small, linear $SiNCS^+$ ion, followed by strong binding to the Au(111) surface. Buried in the bottom of the monolayer, the $SiNCS^+$ ion may be protected against the Xe^+ collisions used for the sputtering analysis.

Conclusions

We investigated the dynamics of collisions of silyl ions ($SiNCS^+$ and $(CH_3)_2SiNCS^+$) with a perfluorinated alkanethiol self-assembled monolayer, as well as the long-time dynamics involved in the thermal desorption of these ions. The short-time collisions dynamics showed similar behavior for both ions. It is predicted that trapping is the most probable event when the incident angle is perpendicular to the surface. The trapping probability decreases substantially when the incident angle is 55º, especially for $(CH_3)_2SiNCS^+$ at 30 eV, for which 9.1% of the trajectories remained trapped during the 60 ps simulation time. Since soft landing was not experimentally observed under the latter conditions, our simulations may overestimate the trapping probabilities.

The residence time of the $SiNCS^+$ ion is always calculated to be significantly shorter than that of $(CH_3)_2SiNCS^+$. We suggest that the experimental observation that soft landing is only observed for the $(CH_3)_2SiNCS^+$ ion is a consequence of different time scales for desorption. Both ions experience soft landing, but for the smaller $SiNCS^+$ ion the residence time is probably too short to be resolved in the experiment. The work reported here illustrates the capability of the BXD method for conducting simulations of dynamic processes occurring on time scales that are difficult to be investigated by brute force molecular dynamics techniques.

The free energy for desorption of the methylated ion is calculated to be 2.4 kcal/mol higher than that of the parent ion. The free energy profiles predict minima around 15 Å, indicating a preference for the ions to be located on the top of the monolayer. The strongest attractive interactions between the ions and the F-SAM are found inside the monolayer (≈ 8 Å), and are predicted to be more important, by about 10 kcal/mol, for the methylated species, in agreement with Cooks' conclusions.[16] However, the entropic contribution to the free energy favors desorption, making it unfavorable the penetration of the ion into the monolayer.

DFT calculations of $SiNCS^+$ and $(CH_3)_2SiNCS^+$ interacting with a Au(111) surface predict that the $SiNCS^+$ ion can be strongly chemisorbed to the gold surface. The ion is positioned perpendicularly to the surface, in a hollow fcc site, forming bonds of 2.38 Å with the three nearest Au atoms. The calculated binding energy is 60 kcal/mol, that is, 10 kcal/mol higher than that estimated for the binding of alkanethiols on gold.[38] The total charges calculated for $SiNCS^+$ and $(CH_3)_2SiNCS^+$ (of +1.12 and +0.62 au, respectively) may suggest that neutralization of the ions is unlikely, especially for $SiNCS^+$. Although the free energy profiles point out that deep penetration of the ions is difficult, the possibility for the small ion to approach the Au(111) surface and get chemisorbed should not be ruled out. If this occurred, the ion might not be sputtered during the Xe^+ bombardment due to the protection of the perfluoroalkane chains.

Acknowledgements

J.J.N., E.M.-N. and S.A.V. are grateful to the "Centro de Supercomputación de Galicia (CESGA)" for the use of its computational resources, as well as to "Ministerio de Economía y Competitividad" (Grant No. CTQ2009-12588) for financial support. D.S. and E.M.-N. acknowledge the Leverhulme Trust for funding the E.M.-N. visit to Leeds by the grant "Accelerated classical and quantum molecular dynamics and its applications" (Grant No. VP1-2012-013). Y.W., F.M. and M.A. acknowledge financial support from Projects FIS2010-15127, CTQ2010-17006, and NANOBIOMAGNET S2009/MAT1726 (CAM program). The contributions of W.L.H for this work were supported by the National Science Foundation under the Partnership in International Research and Education (PIRE) Grant No. OISE-0730114 and the Robert A. Welch Foundation under Grant No. D-0005.

Supporting Information Available

Tables showing the parameters of the intramolecular potentials for the ions, vibrational frequencies of the ions, variation of percentages of trajectory types with h_{limit} for E_i = 10 eV and θ_i = 0º, energy transfer for E_i = 10 eV and θ_i = 0º, box-to-box rate coefficients, and figure showing the survival probability of ions in the F-SAM. This information is available free of charge via the Internet at http://pubs.acs.org.

References

1. Cyriac, J.; Pradeep, T.; Kang, H.; Souda, R.; Cooks, R. G., Low-Energy Ionic Collisions at Molecular Solids. *Chem. Rev.* **2012,** *112*, 5356-5411.
2. Gologan, B.; Green, J. R.; Alvarez, J.; Laskin, J.; Graham Cooks, R., Ion/Surface Reactions and Ion Soft-Landing. *Phys. Chem. Chem. Phys.* **2005,** *7*, 1490-1500.
3. Mitsui, M.; Nagaoka, S.; Matsumoto, T.; Nakajima, A., Soft-Landing Isolation of Vanadium-Benzene Sandwich Clusters on a Room-Temperature Substrate Using N-Alkanethiolate Self-Assembled Monolayer Matrixes. *J. Chem. Phys. B* **2006,** *110*, 2968-2971.
4. Claeyssens, F.; Pratontep, S.; Xirouchaki, C.; Palmer, R. E., Immobilization of Large Size-Selected Silver Clusters on Graphite. *Nanotechnology* **2006,** *17*, 805-807.
5. Nanita, S. C.; Takats, Z.; Cooks, R. G.; Myung, S.; Clemmer, D. E., Chiral Enrichment of Serine Via Formation, Dissociation, and Soft-Landing of Octameric Cluster Ions. *J. Am. Soc. Mass. Spectrom.* **2004,** *15*, 1360-1365.
6. Nagaoka, S.; Ikemoto, K.; Matsumoto, T.; Mitsui, M.; Nakajima, A., Thermal and Hyperthermal Collision-Energy Depositions of Transition Metal-Benzene Sandwich Complexes onto a Self-Assembled N-Octadecanethiol Monolayer. *J. Phys. Chem. C* **2008,** *112*, 6891-6899.
7. Nagaoka, S.; Ikemoto, K.; Matsumoto, T.; Mitsui, M.; Nakajima, A., Soft-Landing Isolation of Gas-Phase-Synthesized Transition Metal-Benzene Complexes into a Fluorinated Self-Assembled Monolayer Matrix. *J. Phys. Chem. C* **2008,** *112*, 15824-15831.
8. Matsumoto, T.; Nagaoka, S.; Ikemoto, K.; Mitsui, M.; Ara, M.; Tada, H.; Nakajima, A., Characterization of Alkyl Monolayer Covalently Bonded to Si(111) and Soft-Landing of Vanadium-Benzene Sandwich Clusters onto the Alkyl Monolayer Substrate. *Eur. Phys. J. D* **2009,** *52*, 99-102.
9. Laskin, J.; Wang, P.; Hadjar, O., Soft-Landing of $Co^{III}(Salen)^{+}$ and $Mn^{III}(Salen)^{+}$ on Self-Assembled Monolayer Surfaces *J. Phys. Chem. C* **2010,** *114*, 5305-5311.
10. Johnson, G. E.; Wang, C.; Priest, T.; Laskin, J., Monodisperse Au_{11} Clusters Prepared by Soft Landing of Mass Selected Ions. *Anal. Chem.* **2011,** *83*, 8069-8072.
11. Johnson, G. E.; Priest, T.; Laskin, J., Coverage-Dependent Charge Reduction of Cationic Gold Clusters on Surfaces Prepared Using Soft Landing of Mass-Selected Ions. *J. Phys. Chem. C* **2012,** *116*, 24977-24986.
12. Franchetti, V.; Solka, B. H.; Baitinger, W. E.; Amy, J. W.; Cooks, R. G., Soft Landing of Ions as a Means of Surface Modification. *Int. J. Mass Spectrom. Ion Phys.* **1977,** *23*, 29-35.
13. Miller, S. A.; Luo, H.; Pachuta, S. J.; Cooks, R. G., Soft-Landing of Polyatomic Ions at Fluorinated Self-Assembled Monolayer Surfaces. *Science* **1997,** *275*, 1447-1450.
14. Johnson, G. E.; Hu, Q.; Laskin, J., Soft Landing of Complex Molecules on Surfaces. *Annu. Rev. Anal. Chem.* **2011,** *4*, 83-104.
15. Verbeck, G.; Hoffmann, W.; Walton, B., Soft-Landing Preparative Mass Spectrometry. *Analyst* **2012,** *137*, 4393-4407.
16. Luo, H.; Miller, S. A.; Cooks, R. G.; Pachuta, S. J., Soft Landing of Polyatomic Ions for Selective Modification of Fluorinated Self-Assembled Monolayer Surfaces. *Int. J. Mass. Spectrom. Ion Proc.* **1998,** *174*, 193-217.
17. Shen, J.; Yim, Y. H.; Feng, B.; Grill, V.; Evans, C.; Cooks, R. G., Soft Landing of Ions onto Self-Assembled Hydrocarbon and Fluorocarbon Monolayer Surfaces. *Int. J. Mass. Spectrom.* **1999,** *182-183*, 423-435.

18. Wijesundara, M. B. J.; Fuoco, E.; Hanley, L., Preparation of Chemical Gradient Surfaces by Hyperthermal Polyatomic Ion Deposition: A New Method for Combinatorial Materials Science. *Langmuir* **2001,** *17*, 5721-5726.
19. Volny, M.; Sengupta, A.; Wilson, C. B.; Swanson, B. D.; Davis, E. J.; Turecek, F., Surface-Enhanced Raman Spectroscopy of Soft-Landed Polyatomic Ions and Molecules. *Anal. Chem.* **2007,** *79*, 4543-4551.
20. Rauschenbach, S.; Vogelgesang, R.; Malinowski, N.; Gerlach, J. r. W.; Benyoucef, M.; Costantini, G.; Deng, Z.; Thontasen, N.; Kern, K., Electrospray Ion Beam Deposition: Soft-Landing and Fragmentation of Functional Molecules at Solid Surfaces. *ACS Nano* **2009,** *3*, 2901-2910.
21. Nie, Z.; Li, G.; Goodwin, M. P.; Gao, L.; Cyriac, J.; Cooks, R. G., In Situ Sims Analysis and Reactions of Surfaces Prepared by Soft Landing of Mass-Selected Cations and Anions Using an Ion Trap Mass Spectrometer. *J. Am. Soc. Mass. Spectrom.* **2009,** *20*, 949-956.
22. Kaiser, B.; Bernhardt, T. M.; Stegemann, B.; Opitz, J.; Rademann, K., Bimodal Distribution in the Fragmentation Behavior of Small Antimony Clusters Sb_x^+ (X=3-12) Scattered from a Highly Oriented Pyrolitic Graphite Surface. *Phys. Rev. Lett.* **1999,** *83*, 2918-2921.
23. Yamaguchi, W.; Yoshimura, K.; Tai, Y.; Maruyama, Y.; Igarashi, K.; Tanemura, S.; Murakami, J., Energy-Controlled Depositions of Size-Selected Silver Nanoparticles on Hopg Substrates. *Chem. Phys. Lett.* **1999,** *311*, 341-345.
24. Messerli, S.; Schintke, S.; Morgenstern, K.; Sanchez, A.; Heiz, U.; Schneider, W.-D., Imaging Size-Selected Silicon Clusters with a Low-Temperature Scanning Tunneling Microscope. *Surf. Sci.* **2000,** *465*, 331-338.
25. Johnson, G. E.; Lysonski, M.; Laskin, J., In Situ Reactivity and Tof-Sims Analysis of Surfaces Prepared by Soft and Reactive Landing of Mass-Selected Ions. *Anal. Chem.* **2010,** *82*, 5718-5727.
26. Gologan, B.; Takáts, Z.; Alvarez, J.; Wiseman, J. M.; Talaty, N.; Ouyang, Z.; Cooks, R. G., Ion Soft-Landing into Liquids: Protein Identification, Separation, and Purification with Retention of Biological Activity. *J. Am. Soc. Mass. Spectrom.* **2004,** *15*, 1874-1884.
27. Alvarez, J.; Futrell, J. H.; Laskin, J., Soft-Landing of Peptides onto Self-Assembled Monolayer Surfaces. *J. Phys. Chem. A* **2006,** *110*, 1678-1687.
28. Volny, M.; Elam, W. T.; Branca, A.; Ratner, B. D.; Turecek, F., Preparative Soft and Reactive Landing of Multiply Charged Protein Ions on a Plasma-Treated Metal Surface. *Anal. Chem.* **2005,** *77*, 4890-4896.
29. Hadjar, O.; Wang, P.; Futrell, J. H.; Laskin, J., Effect of the Surface on Charge Reduction and Desorption Kinetics of Soft Landed Peptide Ions. *J. Am. Soc. Mass. Spectrom.* **2009,** *20*, 901-906.
30. Hu, Q.; Wang, P.; Laskin, J., Effect of the Surface on the Secondary Structure of Soft Landed Peptide Ions. *Phys. Chem. Chem. Phys.* **2010,** *12*, 12802-12810.
31. Ouyang, Z.; Takats, Z.; Blake, T. A.; Gologan, B.; Guymon, A. J.; Wiseman, J. M.; Oliver, J. C.; Davisson, V. J.; Cooks, R. G., Preparing Protein Microarrays by Soft-Landing of Mass-Selected Ions. *Science* **2003,** *301*, 1351-1354.
32. Rauschenbach, S.; Stadler, F. L.; Lunedei, E.; Malinowski, N.; Koltsov, S.; Costantini, G.; Kern, K., Electrospray Ion Beam Deposition of Clusters and Biomolecules. *Small* **2006,** *2*, 540-547.

33. Pepi, F.; Ricci, A.; Tata, A.; Favero, G.; Frasconi, M.; Delle Noci, S.; Mazzei, F., Soft Landed Protein Voltammetry. *Chem. Commun.* **2007**, 3494-3496.
34. Mazzei, F.; Favero, G.; Frasconi, M.; Tata, A.; Tuccitto, N.; Licciardello, A.; Pepi, F., Soft-Landed Protein Voltammetry: A Tool for Redox Protein Characterization. *Anal. Chem.* **2008,** *80*, 5937-5944.
35. Deng, Z.; Thontasen, N.; Malinowski, N.; Rinke, G.; Harnau, L.; Rauschenbach, S.; Kern, K., A Close Look at Proteins: Submolecular Resolution of Two- and Three-Dimensionally Folded Cytochrome C at Surfaces. *Nano Letters* **2012,** *12*, 2452-2458.
36. Feng, B.; Wunschel, D. S.; Masselon, C. D.; Pasa-Tolic, L.; Smith, R. D., Retrieval of DNA Using Soft-Landing after Mass Analysis by Esi-Fticr for Enzymatic Manipulation. *J. Am. Chem. Soc.* **1999,** *121*, 8961-8962.
37. Siuzdak, G.; Bothner, B.; Yeager, M.; Brugidou, C.; Fauquet, C. M.; Hoey, K.; Change, C.-M., Mass Spectrometry and Viral Analysis. *Chem. Biol.* **1996,** *3*, 45.
38. Love, J. C.; Estroff, L. A.; Kriebel, J. K.; Nuzzo, R. G.; Whitesides, G. M., Self-Assembled Monolayers of Thiolates on Metals as a Form of Nanotechnology. *Chem. Rev.* **2005,** *105*, 1103-1170.
39. Miller, S. A.; Luo, H.; Jiang, X.; Rohrs, H. W.; Cooks, R. G., Ion/Surface Reactions, Surface-Induced Dissociation and Surface Modification Resulting from Hyperthermal Collisions of $OCNCO^+$, $OCNCS^+$, $(CH_3)_2SiNCO^+$, and $(CH_3)_2SiNCS^+$ with a Fluorinated Self-Assembled Monolayer Surface. *Int. J. Mass. Spectrom. Ion Proc.* **1997,** *160*, 83-105.
40. Glowacki, D. R.; Paci, E.; Shalashilin, D. V., Boxed Molecular Dynamics: A Simple and General Technique for Accelerating Rare Event Kinetics and Mapping Free Energy in Large Molecular Systems. *J. Chem. Phys. B* **2009,** *113*, 16603-16611.
41. Glowacki, D. R.; Paci, E.; Shalashilin, D. V., Boxed Molecular Dynamics: Decorrelation Time Scales and the Kinetic Master Equation. *J. Chem. Theory Comput.* **2011,** *7*, 1244-1252.
42. Shalashilin, D. V.; Beddard, G. S.; Paci, E.; Glowacki, D. R., Peptide Kinetics from Picoseconds to Microseconds Using Boxed Molecular Dynamics: Power Law Rate Coefficients in Cyclisation Reactions. *J. Chem. Phys.* **2012,** *137*, 165102.
43. Martínez-Núñez, E.; Rahaman, A.; Hase, W. L., Chemical Dynamics Simulations of Co2 Scattering Off a Fluorinated Self-Assembled Monolayer Surface. *J. Phys. Chem. C* **2007,** *111*, 354-364.
44. Vázquez, S. A.; Morris, J. R.; Rahaman, A.; Mazyar, O. A.; Vayner, G.; Addepalli, S. V.; Hase, W. L.; Martínez-Núñez, E., Inelastic Scattering Dynamics of Ar from a Perfluorinated Self-Assembled Monolayer Surface. *J. Phys. Chem. A* **2007,** *111*, 12785-12794.
45. Nogueira, J. J.; Sánchez-Coronilla, A.; Marques, J. M. C.; Hase, W. L.; Martínez-Núñez, E.; Vázquez, S. A., Intermolecular Potentials for Simulations of Collisions of $SiNCS^+$ and $(CH_3)_2SiNCS^+$ Ions with Fluorinated Self-Assembled Monolayers. *Chem. Phys.* **2012,** *399*, 193-204.
46. Grimme, S., Accurate Description of Van Der Waals Complexes by Density Functional Theory Including Empirical Corrections. *J. Comp. Chem.* **2004,** *25*, 1463-1473.
47. Grimme, S., Semiempirical GGA-Type Density Functional Constructed with a Long-Range Dispersion Correction. *J. Comp. Chem.* **2006,** *27*, 1787-1799.
48. Ahlrichs, R.; Bär, M.; Häser, M.; Horn, H.; Kölmel, C., Electronic Structure Calculations on Workstation Computers: The Program System Turbomole. *Chem. Phys. Lett.* **1989,** *162*, 165-169.

49. Wolf, R. J.; Bhatia, D. S.; Hase, W. L., Effect of Bond Stretch Excitation on the Attenuation of Bending Forces. *Chem. Phys. Lett.* **1986,** *132*, 493-497.
50. Curtiss, L. A.; Redfern, P. C.; Raghavachari, K., Gaussian-4 Theory. *J. Chem. Phys.* **2007,** *126*, 084108.
51. Borodin, O.; Smith, G. D.; Bedrov, D., A Quantum Chemistry Based Force Field for Perfluoroalkanes and Poly(Tetrafluoroethylene). *J. Phys. Chem. B* **2002,** *106*, 9912.
52. Buckingham, R. A., The Classical Equation of State of Gaseous Helium, Neon and Argon. *Proc. R. Soc. Lond. A* **1938,** *168*, 264-283.
53. Wang, J.; Hase, W. L., Intermolecular Potential to Represent Collisions of Protonated Peptide Ions with Fluorinated Alkane Surfaces. *J. Chem. Phys. B* **2005,** *109*, 8320-8324.
54. Deb, B.; Hu, W.; Song, K.; Hase, W. L., An Analytical Potential Energy Function to Model Protonated Peptide Soft-Landing Experiments. The Ch3nh3+/Ch4 Interactions. *Phys. Chem. Chem. Phys.* **2008,** *10*, 4565-4572.
55. Vayner, G.; Alexeev, Y.; Wang, J.; Windus, T. L.; Hase, W. L., Ab Initio and Analytic Intermolecular Potentials for Ar-CF_4 *J. Phys. Chem. A* **2005,** *110*, 3174-3178.
56. Alexander, W. A.; Troya, D., Theoretical Study of the Ar-, Kr-, and Xe-Ch4, -Cf4 Intermolecular Potential-Energy Surfaces. *J. Phys. Chem. A* **2006,** *110*, 10834-10843.
57. Alexander, W. A.; Morris, J. R.; Troya, D., Experimental and Theoretical Study of Co Collisions with Ch3- and Cf3-Terminated Self-Assembled Monolayers. *J. Chem. Phys.* **2009,** *130*, 084702.
58. Nogueira, J. J.; Homayoon, Z.; Vázquez, S. A.; Martínez-Núñez, E., Chemical Dynamics Study of No Scattering from a Perfluorinated Self-Assembled Monolayer. *J. Phys. Chem. C* **2011,** *115*, 23817-23830.
59. Monge-Palacios, M.; Nogueira, J. J.; Martínez-Núñez, E., Energy Transfer and Thermal Accommodation in Ozone Scattering from a Perfluorinated Self-Assembled Monolayer. *J. Phys. Chem. C* **2012,** *116*, 25454-25464.
60. Hase, W. L. *Venus 2005*, Venus 2005; Texas Tech University: 2005.
61. Hu, X.; Hase, W. L.; Pirraglia, T., Vectorization of the General Monte Carlo Classical Trajectory Program Venus. *J. Comp. Chem.* **1991,** *12*, 1014-1024.
62. Allen, M. P.; Tildesley, D. J., *Computer Simulation of Liquids*. Clarendon Press: Oxford, 1987.
63. Brooks, B. R.; Bruccoleri, R. E.; Olafson, B. D.; States, D. J.; Swaminathan, S.; Karplus, M., Charmm: A Program for Macromolecular Energy, Minimization, and Dynamics Calculations. *J. Comp. Chem.* **1983,** *4*, 187-217.
64. Brooks, B. R.; Brooks, C. L.; Mackerell, A. D.; Nilsson, L.; Petrella, R. J.; Roux, B.; Won, Y.; Archontis, G.; Bartels, C.; Boresch, S., et al., Charmm: The Biomolecular Simulation Program. *J. Comp. Chem.* **2009,** *30*, 1545-1614.
65. McQuarrie, D. A., *Mathematical Methods for Scientists and Engineers*. University Science Books: Sausalito, California, 2003.
66. Los, J.; Geerlings, J. J. C., Charge Exchange in Atom-Surface Collisions. *Phys. Rep.* **1990,** *190*, 133-90.
67. *Handbook of Chemistry and Physics*. 75th ed.; Ed. D.R. Lide, CRC Press, Boca Raton, Fl, USA: 1995.
68. Perdew, J. P.; Burke, K.; Ernzerhof, M., Generalized Gradient Approximation Made Simple. *Phys. Rev. Lett.* **1996,** *77*, 3865-3868.

69. Kresse, G.; Hafner, J., Ab Initio Molecular-Dynamics Simulation of the Liquid-Metal–Amorphous-Semiconductor Transition in Germanium. *Phys. Rev. B* **1994,** *49*, 14251-14269.
70. Kresse, G.; Furthmüller, J., Efficient Iterative Schemes for Ab Initio Total-Energy Calculations Using a Plane-Wave Basis Set. *Phys. Rev. B* **1996,** *54*, 11169-11186.
71. Kresse, G.; Furthmüller, J., Efficiency of Ab-Initio Total Energy Calculations for Metals and Semiconductors Using a Plane-Wave Basis Set. *Comput. Mater. Sci.* **1996,** *6*, 15-50.
72. Kresse, G.; Joubert, D., From Ultrasoft Pseudopotentials to the Projector Augmented-Wave Method. *Phys. Rev. B* **1999,** *59*, 1758-1775.
73. Blöchl, P. E., Projector Augmented-Wave Method. *Phys. Rev. B* **1994,** *50*, 17953-17979.
74. Methfessel, M.; Paxton, A. T., High-Precision Sampling for Brillouin-Zone Integration in Metals. *Phys. Rev. B* **1989,** *40*, 3616-3621.
75. Monkhorst, H. J.; Pack, J. D., Special Points for Brillouin-Zone Integrations. *Phys. Rev. B* **1976,** *13*, 5188-5192.
76. Bader, R. F. W., Atoms in Molecules. *Acc. Chem. Res.* **1985,** *18*, 9-15.
77. Bader, R. F. W., *Atoms in Molecules: A Quantum Theory*. Oxford University Press: Oxford, UK, 1990.
78. Bader, R. F. W., A Quantum Theory of Molecular Structure and Its Applications. *Chem. Rev.* **1991,** *91*, 893-928.
79. Arnaldsson, A.; Tang, W.; Henkelman, G. *Bader Analysis Program.* *Http://Theory.Cm.Utexas.Edu/Vtsttools/Bader/*.
80. Tasic, U. S.; Yan, T.; Hase, W. L., Dynamics of Energy Transfer in Collisions of O(3p) Atoms with a 1-Decanethiol Self-Assembled Monolayer Surface. *J. Phys. Chem. B* **2006,** *110*, 11863-11877.
81. Nogueira, J. J.; Vázquez, S. A.; Mazyar, O. A.; Hase, W. L.; Perkins Jr., B. G.; Nesbitt, D. J.; Martínez-Núñez, E., Dynamics of CO_2 Scattering Off a Perfluorinated Self-Assembled Monolayer. Influence of the Incident Collision Energy, Mass Effects, and Use of Different Surface Models. *J. Phys. Chem. A* **2009,** *113*, 3850-3865.

82. Nogueira, J. J.; Hase, W. L.; Martínez-Núñez, E., Understanding Energy Transfer in Gas–Surface Collisions from Gas-Phase Models. *J. Phys. Chem. C* **2014,** *118*, 2609-2621.
83. Warmflash, A.; Bhimalapuram, P.; Dinner, A. R., Umbrella Sampling for Nonequilibrium Processes. *J. Chem. Phys.* **2007,** *127*, 154112.
84. Glowacki, D. R.; Liang, C.-H.; Morley, C.; Pilling, M. J.; Robertson, S. H., Mesmer: An Open-Source Master Equation Solver for Multi-Energy Well Reactions. *J. Phys. Chem. A* **2012,** *116*, 9545-9560.

Table 1. Percentages of trajectory types.

	$SiNCS^+$		$(CH_3)_2SiNCS^+$	
	$\theta_i = 0$	$\theta_i = 55$	$\theta_i = 0$	$\theta_i = 55$
		$E_i = 10$ eV		
Direct scattering	7.1	15.8	5.5	13.1
Physisorp.	3.4	57.8	2.5	51.0
Direct-Penet.	76.2	4.3	71.4	3.8
Phys-Penet.	13.3	22.1	20.6	32.1
Trapped	80.4	15.7	86.2	27.1
		$E_i = 30$ eV		
Direct scattering	2.0	13.9	1.6	9.0
Physisorp.	1.0	31.8	0.5	26.5
Direct-Penet.	94.8	14.7	96.4	19.0
Phys-Penet.	2.2	39.6	1.5	45.5
Trapped	67.8	12.6	76.5	9.1

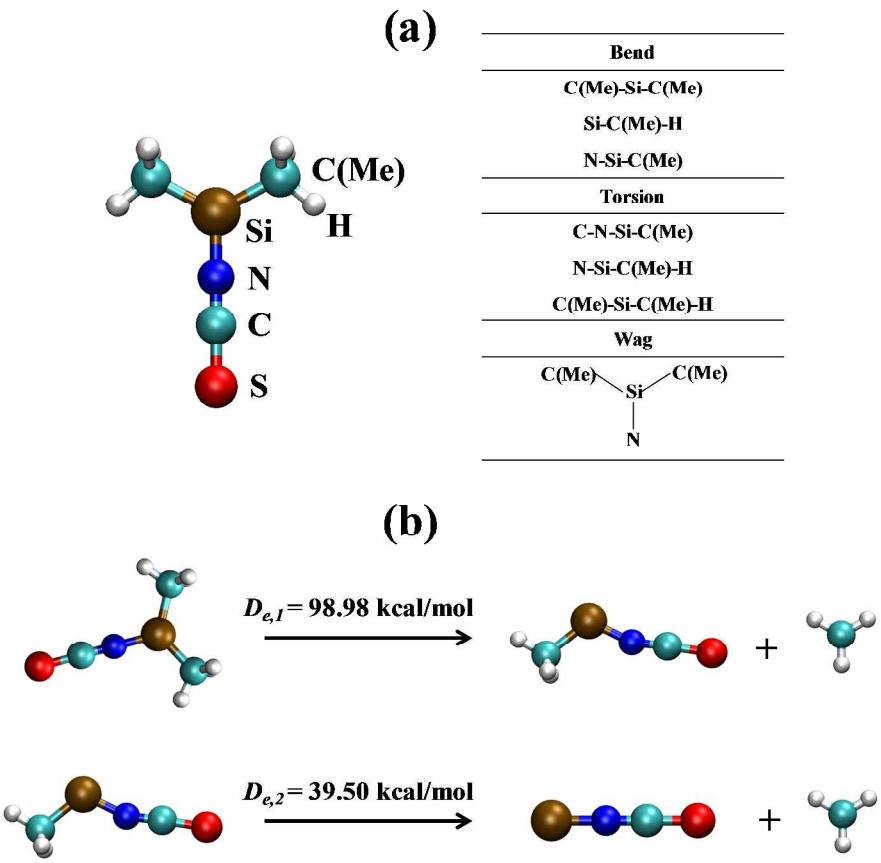

Figure 1: (a) Intramolecular terms that include switching functions. (b) Dissociation of methyl groups showing the equilibrium dissociation energies $D_{e,1}$ and $D_{e,2}$.

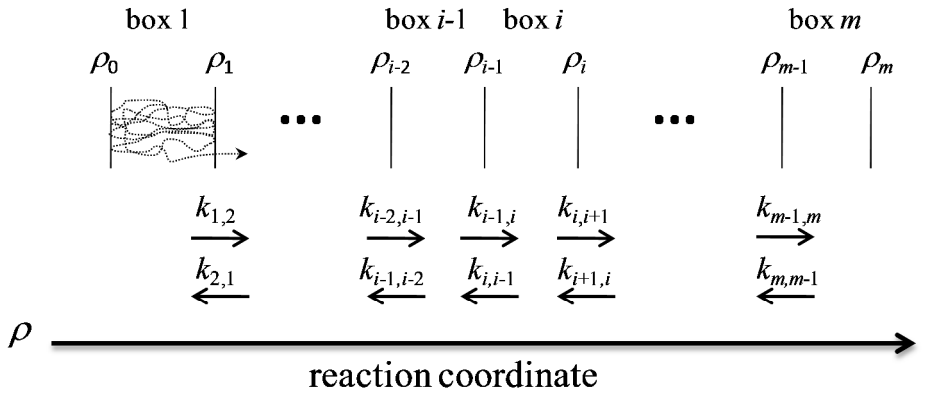

Figure 2: Schematic drawing showing the basis of the BXD method.

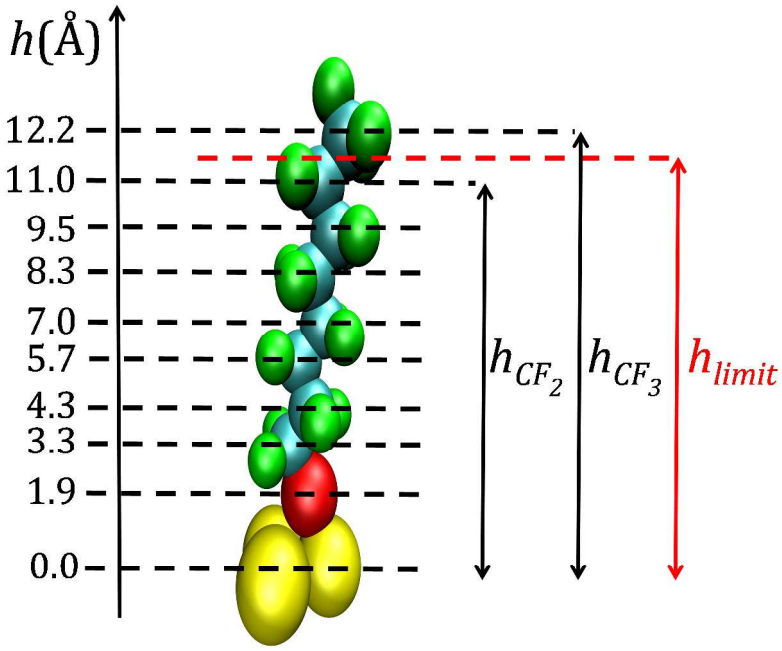

Figure 3: Schematic drawing showing the limiting height used to define penetrating trajectories. The values correspond to average heights of C and S atoms relative to the Au plane.

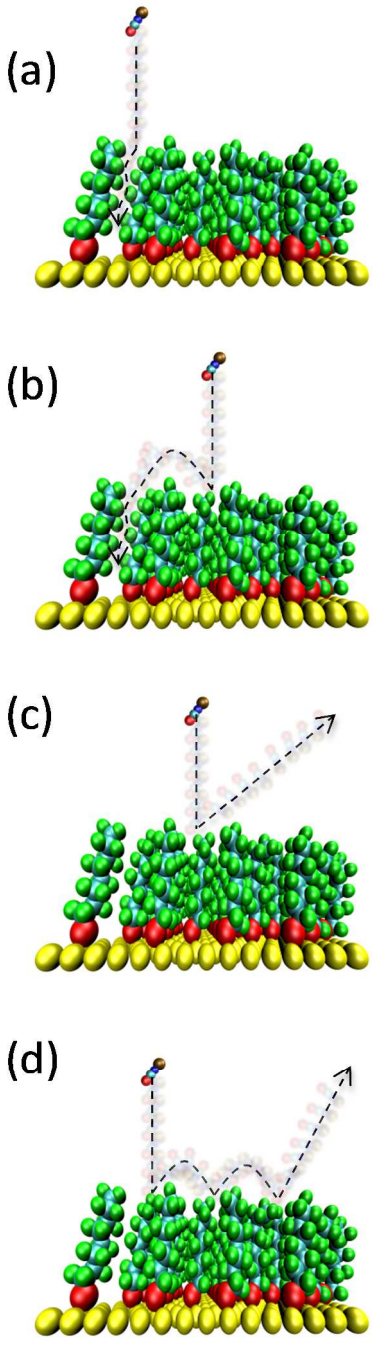

Figure 4: Cartoons showing (a) direct-penetration, (b) physisorption-penetration, (c) direct scattering, and (d) physisorption.

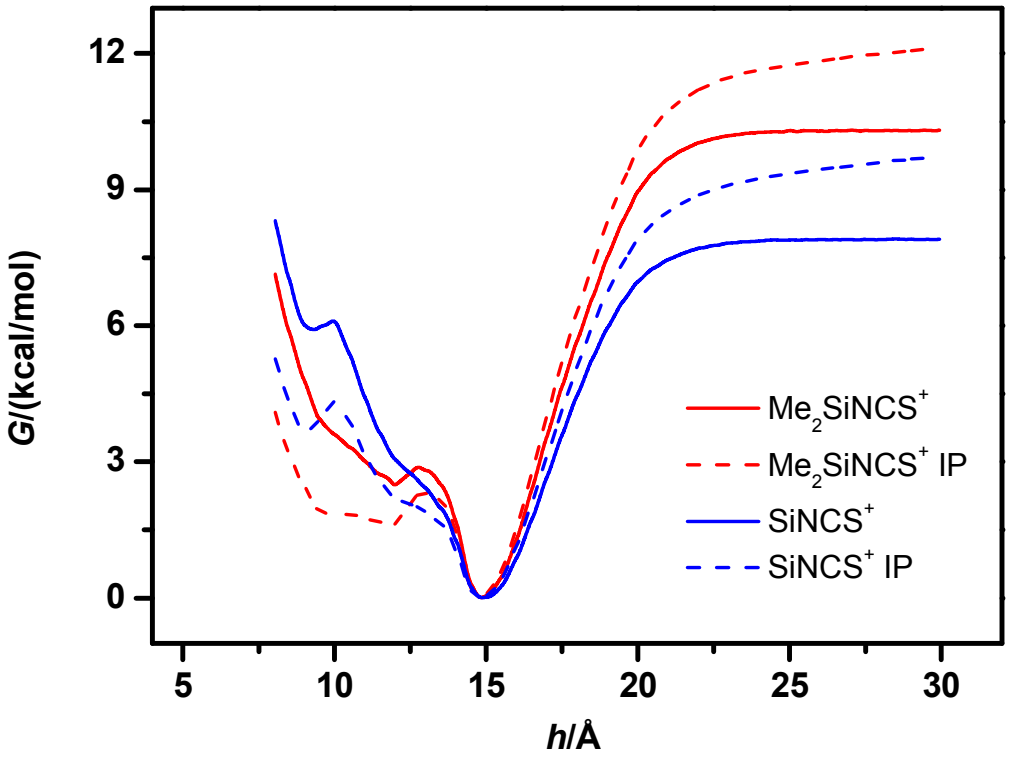

Figure 5: Free energy profiles for desorption of $SiNCS^+$ (blue lines) and Me_2SiNCS^+ (red lines) from F-SAM, with (dashed lines) and without (solid lines) inclusion of the charge image potential.

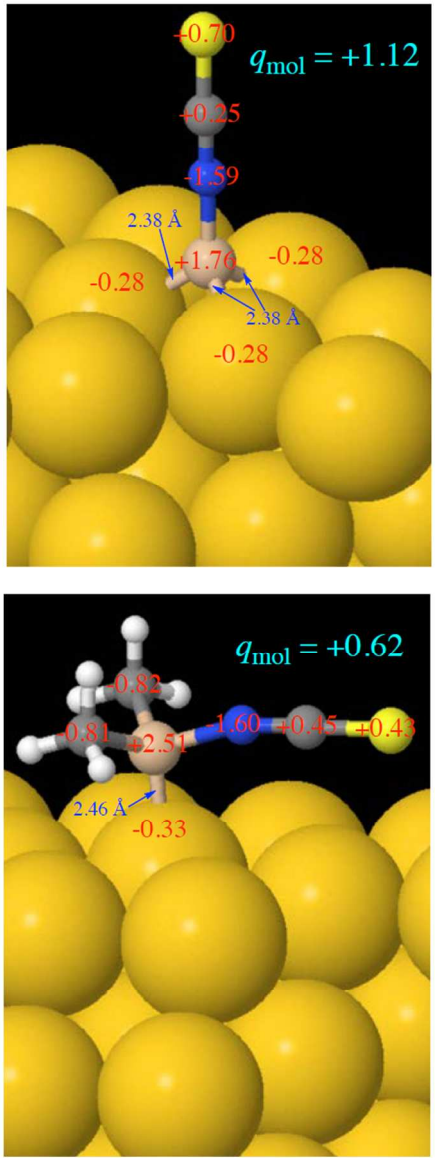

Figure 6: $SiNCS^+$ and $(CH_3)_2SiNCS^+$ interacting with a Au(111) surface. The figures show the QTAIM charges as well as the distances between the Si atoms and the closest Au atoms.

Table of Contents Image

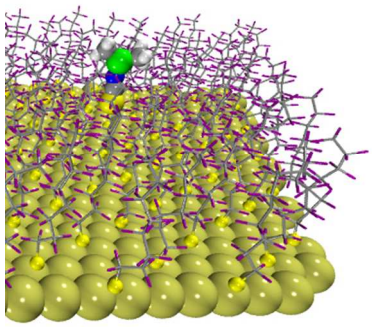

Picture showing the $(CH_3)_2SiNCS^+$ ion trapped in the F-SAM.

Table of Contents Image

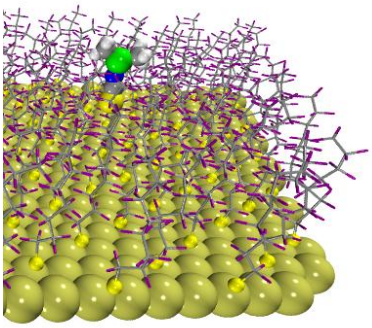

Picture showing the $(CH_3)_2SiNCS^+$ ion trapped in the F-SAM.